Letter

Valley-driven orbital polarization induced by a magnetic impurity in monolayer $NbSe_2$

Amit Chauhan,[1,2,*] Mayank Gupta,[1,2,*] Tapesh Gautam,[1,3,*] B. R. K. Nanda,[1,2,†] and S. Satpathy[1,2,3,‡]

[1]*Condensed Matter Theory and Computational Lab, Department of Physics, IIT Madras, Chennai 600036, India*

[2]*Center for Atomistic Modeling and Materials Design, IIT Madras, Chennai 600036, India*

[3]*Department of Physics & Astronomy, University of Missouri, Columbia, Missouri 65211, USA*

(Received 14 January 2024; revised 28 June 2024; accepted 8 July 2024; published 22 July 2024)

Due to the coupled spin-valley physics, monolayer 2D transition metal dichalcogenides (TMDs) show many unusual electronic and transport properties. Here, we show that a magnetic impurity in the metallic TMDs such as the 2H-$NbSe_2$ induces a large orbital polarization in its neighborhood with a Friedel type oscillation, in addition to the usual spin polarization. We study the orbital polarization, hitherto unexplored for any impurity system, using the impurity Green's function approach as well as tight-binding and density functional methods. Concrete results are presented for the Mn substitutional impurity in $NbSe_2$ from density-functional calculations. The orbital polarization here is due to the orbital moment imbalance between the K/K' valleys, which is driven by the impurity-induced spin imbalance. Our work demonstrates the Friedel oscillation for the first time in the orbital channel. Our results should be readily accessible for experimental study using techniques such as the spin polarized scanning tunneling microscopy.

DOI: 10.1103/PhysRevB.110.L041119

Introduction. It is well known that an impurity center in a metal causes charge fluctuations in the electron gas, giving rise to the characteristic Friedel oscillations [1]. Similarly, a magnetic impurity causes spin polarization (SP) in its neighborhood, which leads to the RKKY interaction between two such magnetic impurities and a flurry of other magnetic phenomena including the Kondo effect. Lesser known is the orbital polarization (OP) that may be produced near the impurity in addition to the SP. For a complete description of magnetism, the OP must also be considered [2]. However, orbital moments in the solid are often quenched or they are small compared to the spin moments [3] and are usually neglected, though in certain solids, especially the f-electron systems, they can be large [4]. When the spin-orbit coupling (SOC) term $\lambda\,\vec{L}\cdot\vec{S}$ is present, electrons in the vicinity of a magnetic impurity acquire both a spin moment and an orbital moment.

Figure 1 illustrates the Friedel oscillations in the orbital channel in the vicinity of a magnetic impurity in $NbSe_2$, which we have obtained from our tight-binding calculations described below. The two-dimensional (2D) monolayer transition metal dichalcogenides (TMDs), of which the 2H-$NbSe_2$ is a member, are of great current interest due to the coupled spin-valley physics. This physics also makes them an excellent system for a potentially large OP near an impurity. This is because there already exists in the pristine system a robust valley-specific orbital moment at the K/K' valleys as illustrated in Fig. 2. Unequal electron occupation of the two valleys due to the exchange coupling with the impurity spin moment can drive a large OP, if conditions are right as discussed below.

Note that in the pristine crystal, while the broken inversion symmetry allows for a nonzero orbital moment at individual k points in the Brillouin zone, the simultaneous presence of the time-reversal symmetry enforces the net orbital moment to be zero, when summed over the Brillouin zone. Addition of a magnetic impurity breaks the time-reversal symmetry, and as a result neither the spin nor the orbital moment is required to be zero anymore.

In this Letter, we show that a magnetic impurity in the TMDs such as 2H-$NbSe_2$ induces a robust OP in its vicinity due to the coupled spin-valley physics. The OP induced by a magnetic impurity should exist to a varying degree in any material with spin-orbit coupling, but could be especially prominent in noncentrosymmetric systems, where orbital moments can exist at individual points in the Brillouin zone in the pristine crystal. The TMDs are particularly well known to have large orbital moments at the valley points K/K', which lead to a robust "valley-driven" OP. Taking the case of 2H-$NbSe_2$ in this family of crystals, as an example, we study the orbital moment formation around a Mn impurity. Based on our results, we suggest the metallic TMDs to be ideal materials to observe the Friedel oscillations in the orbital channel. Our work has added significance in view of the fact that large orbital Hall effects have been predicted in the TMDs [5,6] and other materials [7], and have been observed in several systems recently [8,9].

In order to gain insight into the effect, we first make a back-of-the-envelope estimate of the magnitude of the OP produced at the central site by a magnetic impurity in $NbSe_2$. The band structure, Fig. 2, of the pristine $NbSe_2$ shows hole pockets at K and K', with orbital moments originating from the $L^{\pm} \equiv x^2 - y^2 \pm ixy$ orbitals, while the Γ pocket with z^2 orbital character has no orbital moment and can be ignored. The exchange interaction with the impurity center, $H_{ex} = -J\hat{S}\cdot\hat{s}$, adds a spin-dependent perturbation at the central site.

*These authors contributed equally to this work.

†Contact author: nandab@iitm.ac.in

‡Contact author: SatpathyS@missouri.edu

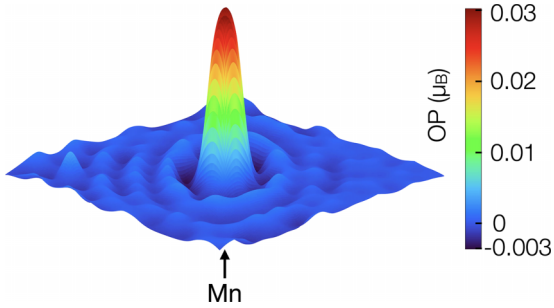

FIG. 1. Computed orbital polarization (OP) in the vicinity of a magnetic impurity in $NbSe_2$ showing the Friedel oscillations.

However, to simplify the estimate, we add this perturbation to every site, which does not change the central site results substantially.

In this approximation, the bands are uniformly shifted. Our theory is valid for both ferromagnetic and antiferromagnetic J. Assuming the former ($J > 0$) for concreteness, the exchange interaction lowers the energy of the spin-up states, so that the $L^+ \uparrow (\downarrow)$ states gain (lose) electrons at the K valley with

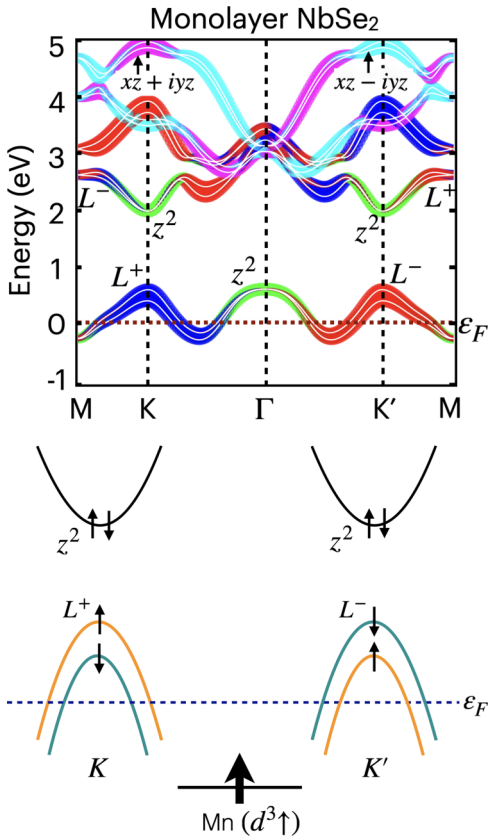

FIG. 2. Top: DFT band structure of the monolayer 2H-$NbSe_2$ with color-coded orbital characters ($L^\pm$ blue/red, z^2 green, $xz + iyz$ purple, and $xz - iyz$ light blue), where $L^\pm \equiv x^2 - y^2 \pm ixy$ and ε_F is the Fermi energy. Bottom: Schematic bands with the hole pockets at the valley points K and K'. The valley-dependent spin splitting is intrinsic to the material without any reference to the impurity. The Mn impurity alters the spin populations differently at the two valleys, causing a net spin and orbital polarization.

the increase given by the integral near the Fermi energy ε_F, viz., $\rho_{+\uparrow} = \int_{\varepsilon_F}^{\varepsilon_F+J} \rho(\varepsilon)\, d\varepsilon$ and $\rho_{+\downarrow} = -\int_{\varepsilon_F-J}^{\varepsilon_F} \rho(\varepsilon + 2\lambda)\, d\varepsilon$, where $\rho(\varepsilon)$ is the density-of-states (DOS) per valley per spin and λ is the strength of the SOC. Note that, in the above integrals, the DOS for the two spin bands are identical, but shifted by the energy splitting 2λ. Similar expressions can be written for $\rho_{-\uparrow}$ and $\rho_{-\downarrow}$ coming from the K' valley for the L_- states, and the net SP/OP due to both valleys can be readily calculated with a Taylor series expansion of the DOS around ε_F. The result is

$$\Delta L_0 = -\lambda J \rho_F' \quad \text{and} \quad \Delta S_0 = J \rho_F, \tag{1}$$

where ΔL_0 (ΔS_0) is the OP (SP) at the central site in contact with the magnetic impurity, ρ_F is the total Fermi energy DOS, including both spins and both valleys, and ρ_F' is its energy derivative.

Though only valid for the central site, Eq. (1) contains the essential points regarding the magnitude of the effect: (i) There is no OP if λ is zero, which is expected; (ii) The OP is much weaker as compared to the SP; and (iii) it disappears if the DOS is flat at the Fermi energy ($\rho_F' = 0$). The ratio is given by $\Delta L_0/\Delta S_0 = -\lambda \rho_F'/\rho_F$. Detailed results [10] show that this ratio computed as a function of λ and J follows Eq. (1) remarkably well and that this ratio is as large as ~25% for the present compounds.

We note that the valley-driven physics of how the impurity-induced OP develops in the TMDs is different from the mechanism of orbital polarization in usual solids. Usually, the magnetic impurity spin polarizes the electron gas, which then due to the SOC leads to OP. However, in the TMDs, intrinsic valley-contrasting orbital moments are already present at the valley points, even without the impurity, due to the inversion symmetry breaking [5]. The SOC then leads in turn to a valley-contrasting spin moment (spin-orbital locking). Time-reversal (TR) symmetry, however, ensures that the net orbital moment is zero, as the opposite orbital moments at the two valleys cancel. When the impurity is introduced, the two valleys are not TR connected anymore, and a net spin imbalance is produced due to the exchange interaction. Since the valley states are spin-orbital locked, the spin imbalance leads to an orbital imbalance, resulting in a net OP.

We have studied the OP quantitatively using three complementary methods: (i) A realistic tight-binding Hamiltonian to study the effects of various interaction parameters, (ii) density functional theory (DFT) calculations taking Mn doped $NbSe_2$ as an example, and (iii) the impurity Green's function approach using the low-energy Hamiltonian, which yields the long-distance behavior.

Tight binding model. We consider the tight-binding (TB) Hamiltonian for the Nb d electrons with a large $NbSe_2$ supercell (up to 21 × 21 f.u.). An exchange interaction J is added to the central Nb site to model the magnetic impurity, so that the Hamiltonian is

$$\mathcal{H} = \sum_{ns\sigma} \varepsilon_s n_{ns\sigma} + \sum_{\langle nn' \rangle ss'\sigma} t_{ns,n's'} (c^\dagger_{ns\sigma} c_{n's'\sigma} + \text{H.c.}) + \lambda\, \vec{L} \cdot \vec{S} - J \sum_s (n_{0s\uparrow} - n_{0s\downarrow}), \tag{2}$$

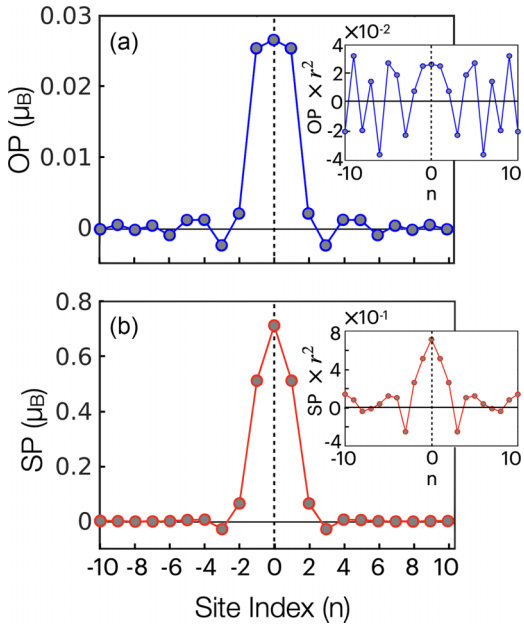

FIG. 3. Orbital and spin polarization along the zigzag direction in $NbSe_2$ from the TB Hamiltonian Eq. (2) with the impurity potential $J = 1$ eV and $J' = 0.5$ eV. Both OP and SP show oscillatory behavior, with the amplitudes falling off roughly as r^{-2}. Insets show the OP/SP, which are multiplied by r^2 except for the impurity site ($r = 0$).

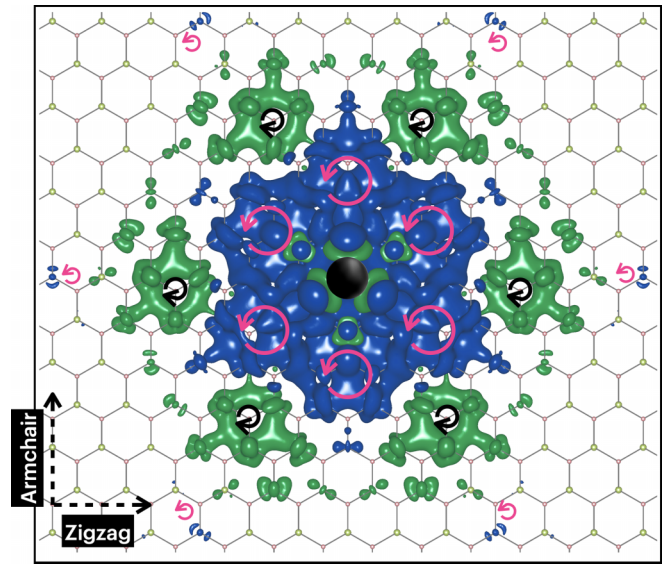

FIG. 4. OP/SP near a Mn impurity in 2H-$NbSe_2$ from DFT. The SP is shown by the color-coded spin density contours, blue/green for spin up/down, while the OP is indicated by the colored circles (L^+ counter-clockwise and L^- clockwise), with the circle size proportional to the magnitude of the OP. In this figure and in Fig. 5, the sign of the impurity Mn moment (black dot at the center) is negative or spin down.

where $c^\dagger_{ns\sigma}$ creates an electron, with n, s, σ being the site, orbital, and spin indices, $n_{ns\sigma}$ is the number operator, ε_s is the on-site orbital energy, λ is the strength of the SOC, and the last term describes the exchange interaction with the magnetic atom. We also considered an additional 1NN exchange interaction, $-J' \sum_{pm} (n_{pm\uparrow} - n_{pm\downarrow})$, where p is summed over the 1NN of the central site, and m is the orbital index, to model the DFT results better. The typical exchange interaction is $J \approx 1$ eV, while J' is a few tenths of an eV. We kept the minimal number of basis set, viz., $|z^2\rangle$, $|xy\rangle$, and $|x^2 - y^2\rangle$ orbitals, and followed a symmetry-based approach [17,18] to construct the TB Hamiltonian in the momentum space, keeping up to the 3NN hopping. The advantage of this approach is that the full symmetry of the structure is incorporated, though the ligand orbitals are not explicitly included in the Hamiltonian. The TB parameters were obtained by fitting to the DFT results for the monolayer $NbSe_2$ (see the Supplemental Material [10] for details).

We diagonalized the TB Hamiltonian Eq. (2) and obtained the site-specific spin/orbital occupancies $\rho_n^{l\sigma}$ by summing over the occupied eigenstates $\psi_{k\nu}$: $\rho_n^{l\sigma} = \sum_{k\nu}^{\text{occ}} |\langle nl\sigma|\psi_{k\nu}\rangle|^2$, where k is the Bloch momentum, ν is the band index, n is the site index, $l = L^+, L^-$, or z^2, and $\sigma = \uparrow$ or $\downarrow$. The site-specific SP/OP are then given by

$$\Delta S_n = \left(\rho_n^{L^+\uparrow} + \rho_n^{L^-\uparrow} + \rho_n^{z^2\uparrow}\right) - \left(\rho_n^{L^+\downarrow} + \rho_n^{L^-\downarrow} + \rho_n^{z^2\downarrow}\right),$$
$$\Delta L_n = \left(\rho_n^{L^+\uparrow} + \rho_n^{L^+\downarrow}\right) - \left(\rho_n^{L^-\uparrow} + \rho_n^{L^-\downarrow}\right). \quad (3)$$

The computed values of ΔS_n and ΔL_n from the TB model are shown in Figs. 1 and 3, which show a robust OP including the Friedel oscillations, with the amplitude falling off as $\sim r^{-2}$. The polarizations are entirely due to the magnetic impurity, as symmetry dictates that for the pristine crystal, both OP and SP are zero, though nonzero polarizations can exist in different parts of the BZ.

Density functional results. As a concrete example, using DFT and supercell geometry, we studied the orbital polarization in the neighborhood of a Mn impurity in $NbSe_2$. A large supercell, $(NbSe_2)_{17\times17}$/Mn, where a single Mn atom replaced the central Nb atom was used. The DFT calculations were performed with the projector augmented wave (PAW) [19] method as implemented in the Vienna *ab initio* simulation package (VASP) [20], using the generalized gradient approximation (GGA) for the exchange-correlation functional. The computed band structure (see the Supplemental Material [10] for details) shows that the Mn atom has Mn($d^3\uparrow$) configuration, with its energy deep below ε_F, occurring in the Se (p) manifold of bands. Its role, therefore, is to simply provide an exchange energy term to the partially filled Nb(d^2) valence states, as captured in the TB model, Eq. (2).

The computed OP/SP near the impurity site is shown in Figs. 4 and 5. The SP/OP in the immediate proximity of the impurity is opposite to the impurity Mn moment due to the antiferromagnetic exchange interaction. From Fig. 5, we see that for the various sites, OP is roughly proportional to the SP, as suggested from Eq. (1), and the ratio between them $\Delta L_n/\Delta S_n$ is as large as 25%, which is remarkably high as compared to the typical 3–5% in the bulk 3*d* crystals such as Fe, Co, and Ni [2,3]. The predicted large value makes these systems ideal candidates for the experimental observation of the OP. We note that because of system size limitations, explicit DFT results for the Friedel oscillations have been obtained so far only in quasi-1D systems to our knowledge, viz., near metal

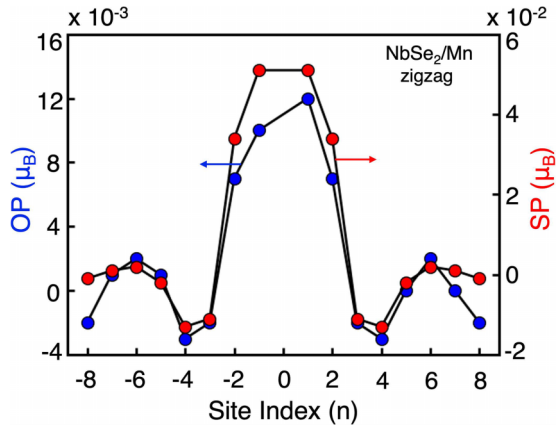

FIG. 5. DFT results for the orbital and spin polarization computed for the $NbSe_2$/Mn along the zigzag chain using a 17×17 supercell, showing Friedel oscillations and a robust OP which is about 25% of the SP.

surfaces along the normal direction [21]. Our results presented here are the first DFT results of Friedel oscillations in dimensions higher than 1D. This is also the first study of the Friedel oscillation in the orbital channel.

Impurity Green's function. Although the DFT results in Fig. 5 already show the oscillatory behavior close to the impurity, one can not go to larger distances due to the system size limitations as mentioned above. In order to study the long-range behavior of the OP, we have used the impurity Green's function approach for the well known valley orbital model [22]. This low energy Hamiltonian model describes the band structure at the valley points quite well, but it is not designed for the Γ point bands. However, the Γ point is not important for the OP, because the hole pocket at Γ has largely z^2 character with zero orbital momentum. The valley orbital model Hamiltonian reads

$$\mathcal{H}_0(\vec{q}) = \vec{d} \cdot \vec{\sigma} + \frac{\tau\lambda}{2}(\sigma_z + 1)s_z, \tag{4}$$

where $\vec{s}$ is the electron spin and $\vec{\sigma}$ is the orbital pseudospin with $|u\rangle = L^\tau \equiv (\sqrt{2})^{-1}(|x^2 - y^2\rangle + i\tau|xy\rangle)$ and $|d\rangle = |z^2\rangle$, $\tau = \pm 1$ is the valley index for K and K' valleys, λ is the SOC constant, $d_x = \tau t q_x a$, $d_y = -t q_y a$, and $d_z = -\Delta/2$, where a is the lattice constant, Δ is the energy gap, t is an effective hopping integral, and momentum $\vec{q}$ is measured with respect to the valley point K or K'. For $NbSe_2$, parameters are [23] $a = 3.45$ Å, $t = -0.8$ eV, $\Delta = 1.3$ eV, and $\lambda = 0.075$ eV. We add a magnetic perturbation at the central site $V_{ns,n's'} = V_s\ \delta_{n0}\delta_{n'0}, \delta_{ss'}$, where n/s are the site/orbital indices. With $H_{ex} = -J\hat{S} \cdot \hat{s}$ added to the central site, the perturbing potential is

$$V_{0s,0s'} = \begin{bmatrix} -J & 0 & 0 & 0 \\ 0 & -J & 0 & 0 \\ 0 & 0 & J & 0 \\ 0 & 0 & 0 & J \end{bmatrix}, \tag{5}$$

where the basis $s = |u\uparrow\rangle, |d\uparrow\rangle, |u\downarrow\rangle$, and $|d\downarrow\rangle$, and u/d denotes the orbital pseudospin states.

We are interested in the site and orbital projected DOS, which can be obtained from the imaginary part of the Green's function: $\rho_n^s(E) = -\pi^{-1}\mathrm{Im}\ G_{ns,ns}(E)$, where $G(E) = (E + i\eta - \mathcal{H})^{-1}$ and $\mathcal{H} = \mathcal{H}_0 + V$. From the Dyson's equation, we have $G = G_0 + G_0 V G$, where G_0 is the unperturbed Green's function. In the real-space basis, its matrix elements can be computed from the eigenstates $(\varepsilon_{\vec{k}\nu}, \phi^s_{\vec{k}\nu})$:

$$G^0_{ns,n's'}(E) = \frac{1}{N}\sum_{\vec{k}\nu} \frac{\phi^{s'*}_{\vec{k}\nu}\, \phi^s_{\vec{k}\nu}\, e^{i\vec{k}\cdot(\vec{R}_n - \vec{R}_{n'})}}{E - \varepsilon_{\vec{k}\nu} + i\eta}, \tag{6}$$

where $\vec{R}_n$ denote the lattice vectors. Since the perturbation V is diagonal and on a single site, the diagonal elements of G needed for the calculation of $\rho_n^s(E)$, assume a simple form:

$$G_{ns,ns} = G^0_{ns,ns} + \begin{bmatrix} V_1 G^0_{ns,01} & V_2 G^0_{ns,02} & V_3 G^0_{ns,03} & V_4 G^0_{ns,04} \end{bmatrix} \begin{bmatrix} 1 - g_{11} & g_{12} & g_{13} & g_{14} \\ g_{21} & 1 - g_{22} & g_{23} & g_{24} \\ g_{31} & g_{32} & 1 - g_{33} & g_{34} \\ g_{41} & g_{42} & g_{43} & 1 - g_{44} \end{bmatrix}^{-1} \begin{bmatrix} G^0_{01,ns} \\ G^0_{02,ns} \\ G^0_{03,ns} \\ G^0_{04,ns} \end{bmatrix}, \tag{7}$$

where $g_{ss'} \equiv V_{s'} G^0_{0s,0s'}$, $V_1 = V_2 = -J$, and $V_3 = V_4 = J$. If the crystal has no virtual or localized states, in the weak-coupling limit, the 4×4 matrix above can be replaced by unity, so that $G_{ns,ns} = G^0_{ns,ns} + \sum_{s'} V_{s'}\ G^0_{ns,0s'}\ G^0_{0s',ns}$. However, in 1D or 2D, bound states occur even with the smallest perturbation, so that one must use the full equation Eq. (7). With our central-site potential, which is attractive for the spin up channel and repulsive for the spin down channel, a resonant state occurs in the spin up channel (see the SM [10] for more details). The site-orbital occupation is simply the imaginary part of the full GF, integrated to the Fermi energy, $\rho_n^s = \int_{-\infty}^{\varepsilon_F} \rho_n^s(E)\, dE$, from which the OP is computed using Eq. (3). Results are shown in Fig. 6, which indicates a robust OP with the Friedel oscillations with an oscillation period of π/k_F, similar to the well-known Friedel oscillations in the charge and spin channels.

In conclusion, we have studied the orbital polarization in the vicinity of a magnetic impurity in the metallic TMDs and predicted a robust orbital polarization together with characteristic Friedel oscillations, which fall off as $\sim r^{-2}$ with distance. The effect is large because in this noncentrosymmetric system, large orbital moments are already present at the valley points of the Brillouin zone in the pristine material. The magnetic impurity induces spin polarization in its vicinity due

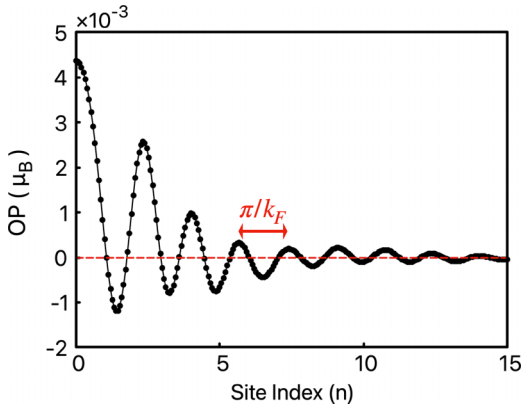

FIG. 6. Friedel oscillations of the OP along the zigzag direction, computed from the impurity Green's function for the valley orbital model, Eq. (4), with the exchange parameter $J = 5\,\mathrm{eV}$.

to exchange coupling via spin imbalance at the two valleys, which in turn leads to the orbital polarization due to the spin-orbit coupling term. The effect was modeled by considering the electronic structure at the K/K' valley points using the low-energy valley-orbital model. A concrete example of a Mn substitutional impurity in the $NbSe_2$ TMD was studied from a supercell density functional calculation, which yielded a large ($\Delta L_n/\Delta S_n \sim 25\%$) orbital polarization in the vicinity of the impurity. Experimental measurement of the effect using spin polarized scanning tunneling microscopy and magnetic exchange force microscopy [24,25] or other techniques would be important to advance the field.

Acknowledgments. This work was funded by the Department of Science and Technology, India, through Grant No. CRG/2020/004330. S.S. thanks the United States-India Educational Foundation (USIEF) for their support through a Fulbright-Nehru Fellowship, jointly funded by the Governments of India and the United States.

[1] J. Friedel, Electronic structure of primary solid solutions in metals, Adv. Phys. **3**, 446 (1954).

[2] T. Thonhauser, Theory of orbital magnetization in solids, Int. J. Mod. Phys. B **25**, 1429 (2011).

[3] A. J. P. Meyer and G. Asch, Experimental g' and g values of Fe, Co, Ni, and their alloys, J. Appl. Phys. **32**, S330 (1961).

[4] M. S. S. Brooks and P. J. Kelly, Large orbital-moment contribution to 5*f* band magnetism, Phys. Rev. Lett. **51**, 1708 (1983).

[5] S. Bhowal and S. Satpathy, Intrinsic orbital moment and prediction of a large orbital Hall effect in two-dimensional transition metal dichalcogenides, Phys. Rev. B **101**, 121112(R) (2020); Intrinsic orbital and spin Hall effects in monolayer transition metal dichalcogenides, **102**, 035409 (2020).

[6] L. M. Canonico, T. P. Cysne, A. Molina-Sanchez, R. B. Muniz, and T. G. Rappoport, Orbital Hall insulating phase in transition metal dichalcogenide monolayers, Phys. Rev. B **101**, 161409(R) (2020).

[7] T. Tanaka, H. Kontani, M. Naito, T. Naito, D. S. Hirashima, K. Yamada, and J. Inoue, Intrinsic spin Hall effect and orbital Hall effect in 4*d* and 5*d* transition metals, Phys. Rev. B **77**, 165117 (2008).

[8] I. Lyalin, S. Alikhah, M. Berritta, P. M. Oppeneer, and R. K. Kawakami, Magneto-optical detection of the orbital Hall effect in chromium, Phys. Rev. Lett. **131**, 156702 (2023).

[9] Y.-G. Choi, D. Jo, K.-H. Ko, D. Go, K.-H. Kim, H. G. Park, C. Kim, B.-C. Min, G.-M. Choi, and H.-W. Lee, Observation of the orbital Hall effect in a light metal Ti, Nature (London) **619**, 52 (2023).

[10] See Supplemental Material at http://link.aps.org/supplemental/10.1103/PhysRevB.110.L041119 for details of the TB model, density-functional results for the Mn impurity in $NbSe_2$, bound state formation in the spin channel, and dependence of OP/SP on SOC and exchange parameters, which also contain Refs. [11–16].

[11] B. R. K. Nanda, M. Sherafati, Z. S. Popović, and S. Satpathy, Electronic structure of the substitutional vacancy in graphene: density-functional and Green's function studies, New J. Phys. **14**, 083004 (2012).

[12] L. F. Mattheiss, Band structures of transition-metal-dichalcogenide layer compounds, Phys. Rev. B **8**, 3719 (1973).

[13] L. A. M. Junior and A. Bruno-Alfonso, Thirteen-band tight-binding model for the MoS_2 monolayer, Mater. Res. **24**, e20210059 (2021).

[14] J. C. Slater and G. F. Koster, Simplified LCAO method for the periodic potential problem, Phys. Rev. **94**, 1498 (1954).

[15] W. A. Harrison, *Electronic Structure and the Properties of Solids: The Physics of the Chemical Bond* (Dover Publications, New York, 1989).

[16] O. K. Andersen and T. Saha-Dasgupta, Muffin-tin orbitals of arbitrary order, Phys. Rev. B **62**, R16219 (2000).

[17] G. B. Liu, W. Y. Shan, Y. Yao, W. Yao, and D. Xiao, Three-band tight-binding model for monolayers of group-VIB transition metal dichalcogenides, Phys. Rev. B **88**, 085433 (2013).

[18] K. V. Shanavas and S. Satpathy, Effective tight-binding model for MX_2 under electric and magnetic fields, Phys. Rev. B **91**, 235145 (2015).

[19] P. E. Blöchl, Projector augmented-wave method, Phys. Rev. B **50**, 17953 (1994).

[20] G. Kresse and J. Furthmüller, Efficient iterative schemes for *ab initio* total energy calculations using a plane-wave basis set, Phys. Rev. B **54**, 11169 (1996).

[21] J.-H. Cho, Ismail, Z. Zhang, and E. W. Plummer, Oscillatory lattice relaxation at metal surfaces, Phys. Rev. B **59**, 1677 (1999); Y. Y. Sun, A. C. H. Huan, Y. P. Feng, and A. T. S. Wee, Reduction of amplitude and wavelength of Friedel oscillation on Na(111) surface, *ibid.* **72**, 153404 (2005); Y. Jia, B. Wu, C. Li, T. L. Einstein, H. H. Weitering, and Z. Zhang, Strong quantum size effects in Pb(111) thin films mediated by anomalous friedel oscillations, Phys. Rev. Lett. **105**, 066101 (2010); J. M. Li, J. Wang, Q. Sun, and Y. Jia, First-principles study of Friedel oscillations normal to the low index surfaces of Al, Phys. B: Condens. Matter **406**, 2767 (2011).

[22] D. Xiao, G.-B. Liu, W. Feng, X. Xu, and W. Yao, Coupled spin and valley physics in monolayers of MoS_2 and other group-VI dichalcogenides, Phys. Rev. Lett. **108**, 196802 (2012).

[23] S. Bhowal and S. Satpathy, Orbital gyrotropic magneto-electric effect and its strain engineering in monolayer NbX_2, Phys. Rev. B **102**, 201403(R) (2020).

[24] R. Wiesendanger, Spin mapping at the nanoscale and atomic scale, Rev. Mod. Phys. **81**, 1495 (2009).

[25] H. Oka, O. O. Brovko, M. Corbetta, V. S. Stepanyuk, D. Sander, and J. Kirschner, Spin-polarized quantum confinement in nanostructures: scanning tunneling microscopy, Rev. Mod. Phys. **86**, 1127 (2014).